DIGITAL ELEVATION MODELS DERIVED FROM SMALL FORMAT LUNAR IMAGES

MARK ROSIEK
Physical Scientist
mrosiek@usgs.gov

Randy Kirk
Geophysicist

Annie Howington-Kraus
Cartographer

United States Geological Survey, Astrogeolgy Program
2255 N. Gemini Dr.
Flagstaff AZ 86001

ABSTRACT

This paper provides a synopsis of a project to collect digital elevation models (DEM) from Clementine imagery. The DEM coverage areas are the lunar north pole (63ºN to 90ºN) and south pole (63ºS to 90ºS). The goals were: (1) provide topographic information where the Clementine altimeter was unable to collect data; (2) provide higher resolution DEMs; (3) have the topographic information align with the Clementine Global Mosaic; and (4) provide topographic information coincident with the boundaries of the quadrangle scheme used for the Clementine Global Mosaic. Work was first carried out on the south pole area. There were many tests and problems with collecting the elevation data. This paper provides the background on the data used to complete this work, a summary of the problems with the different attempts that were made until a successful procedure was developed, and a summary of the current results.

Mapping of the polar areas is clearly of the highest scientific priority because the stereo data can be used to fill the holes in the Clementine altimeter dataset and because of the possibility that volatiles may be trapped in permanently shadowed regions.

This work was completed using a softcopy photogrammetric system, SOCET SET from LH Systems. Any use of trade, product, or firm names is for descriptive purposes only and does not imply endorsement by the U.S. Government.

BACKGROUND

Clementine Mission

The Clementine mission was conceived in 1992 by the National Aeronautics and Space Administration (NASA), U.S. Department of Defense, and industry to test new lightweight spacecraft technology. The goal was to acquire data that would assist in determining the mineral content of the moon and a near-Earth asteroid. In 1994, the Clementine spacecraft acquired digital images of the moon at visible and near infrared wavelengths [Nozette et al. 1994]. On board there were four camera systems and a laser altimeter. During the first month, periapsis was at 30˚S and the highest resolution images were obtained in the southern hemisphere [Cook et al. 1996]. Over the northern polar area a series of oblique and nadir images was obtained with the ultraviolet-visible (UVVIS) camera on each orbit. During the second month, periapsis was at 30˚N and image acquisition was reversed, with high-resolution images in the north and oblique and nadir images in the south.

The four camera systems were an ultraviolet-visible (UVVIS) camera, a long-wave infrared (LWIR) camera, the laser-ranger (LIDAR) high-resolution (HIRES) camera, and a near-infrared (NIR) camera. There were five spectral bands and one broad band that could be selected on the UVVIS camera. The HIRES camera had five spectral bands to select and the NIR camera had six spectral bands to select. The combination of cameras and filters resulted in nearly 1 million images in the 11 visible and near-infrared spectral bands, 620,000 high-resolution images and 320,000 long-wave infrared images.

Altimeter: The LIDAR system was sighted through the HIRES camera optics. The laser return pulses were binned into 40 m segments. Additional errors in determining elevation from LIDAR include orbit repeatability, estimates in the lunar geoid, spacecraft pointing, range jitter, surface roughness, and range walk. An error estimate for laser data is between 100 and 130 m. Altimeter data were collected between 79˚S and 81˚N. The spacing of the data varied. Along-track, over some smooth mare surfaces, an along-track spacing of 20 km was achieved. Where the instrument lost lock over some rough highland terrain the spacing degraded to 100 km. The across-track spacing was based on the orbital track and is approximately 60 km at the equator and less elsewhere. A filter was applied to LIDAR data to reduce the range information to a single range value for each bounce point. The filtered data was then interpolated to fill in the polar regions where the altimeter did not collect data. A global topography model was then derived based on spherical harmonic expansion [Smith et al. 1997, Zuber et al. 1994]. The Clementine LIDAR

topography data and documentation can be downloaded from the Geophysics Subnode of the PDS Geosciences Node (http://pds-geophys.wustl.edu/pds/clementine/).

Image Mosaic: A global image mosaic of the moon was produced from the UVVIS 750 nm Clementine data. Match points were picked to tie the imagery together, and the camera pointing angles were adjusted to align the imagery. This adjustment used a spherical surface, and the elevation for tie points was held to a constant value, 1737.4 km. This produced a seamless image mosaic with latitude and longitude information but no information on the elevation [Eliason et al.1999, Eliason 1997, Isbell et al.1999, Isbell et al.1997]. This mosaic will be used as a base to align the imagery for the other spectral bands of the UVVIS and NIR cameras. This multispectral mosaic then can be used in mineral studies of the lunar surface. Additional information on Clementine can be found at http://wwwflag.wr.usgs.gov/USGSFlag/Space/clementine/clementine.html or http://www-pdsimage.jpl.nasa.gov/PDS/public/Atlas/ .

Other sources of topography data

Thomas de la Rue acquired the first stereoscopic picture of the moon between 1857 and 1860. The stereoscopic effect was achieved by waiting a few years between pictures and using the moon's libration for the stereo view [Sanders 1945].

Methods to collect lunar topography from Earth-based observations include limb profiles, ground-based photogrammetry, and radar interferometry. During the Apollo missions, altimeters and photographic camera systems provided data for topographic studies [Smith et al.1997, Cook et al.2000]. Studies that are more recent have used radar interferometry and Clementine imagery.

Topographic depression could provide a cold trap for volatiles on the lunar surface so radar interferometry was used in searching for possible water ice near the lunar south pole [Margot et al.1998, Margot et al.1999A, Margot et al.1999B]. They were able to obtain high spatial resolution (150 m) with a height resolution of ~50 m. Their technique uses a 70 m radar antenna to transmit a 3.5 cm wavelength signal that is received by two nearby 35 m antennas. The interferometry information is used to derive relative height information that is tied to Clementine altimetry topography.

Topographic data were derived from overlapping nadir images collected by Clementine [Cook et al.1996, Cook and Robinson 1999, Cook et al.2000, Oberst et al.1996]. This technique used stereo models formed by the imagery side lap of images from adjacent orbits. A relative elevation was derived at 1 km spacing and then the digital elevation model (DEM) was adjusted to fit the altimetry data or previously collected photogrammetric topographic data. For the south pole the standard deviation between the adjusted elevations and the Clementine laser altimeter points was ± 0.69 km and for the north pole the standard deviation was ± 0.37 km.

METHODS

Data selection

Imagery: The Clementine mission collected over two million images. Fortunately, a previous project used the images to create a global mosaic and organized information about the images into a database. This information was used to select the images for the polar regions. The UVVIS imagery was most appropriate for the topographic mapping. The camera system also acquired images in a high and low gain setting. The database contained information indicating if the high or low gain image was easier to view. Other information that was useful was time of acquisition, orbit, ground sample distance, latitude and longitude of center point, and the emission angle (an angle between a local surface normal and a vector to the camera system).

The UVVIS camera acquired stereomultispectral imagery that is suitable for determining topography. In addition to global coverage with nadir-looking images, Clementine obtained oblique images of a substantial portion of the moon. During systematic mapping, every other orbit included poleward-looking oblique imaging (covering the north pole in the first month and the south pole in the second).

The UVVIS camera image size was 384x288 pixels with five spectral bands and one broad band. The 750 nm band oblique/nadir pairs were the primary image source for this study. On an oblique image the ground sample distance (GSD) ranged from 300 to 400 meters. The GSD for the nadir images acquired at the end of an orbit were slightly larger and ranged from 325 to 450 meters. Using the formula for stereo height accuracy [Cook et al. 1996] an estimate of height accuracy is 180 m. This formula is IFOVmax/(K·B/H) with IFOVmax defined as Maximum Instantaneous Field of View, B/H is the base-to-height ratio, and K is an estimate of pixel measurement accuracy on the imagery.

Match points: During production of the global mosaic, points were selected to tie one image to another. The points were selected to match adjacent images together within an orbit, then to match images between orbits together, and finally to match images acquired in month one and two together. These points were not transferred to all overlapping images. The match point and camera information were adjusted to a spherical surface. This resulted in revised camera pointing angles and allowed the images to be mosaicked into a near seamless mosaic with a ground sample distance of 100 m for each pixel. The global mosaic has an absolute positional accuracy of better than 0.5 km/pixel; for 95% of the surface [Eliason et al. 1999]. Information on the match point identification, the two image files associated with a match point, and the image coordinates were saved in a file and were available for use in the analytical triangulation. This information made it easy to use these match points as horizontal control.To use the match points as vertical control a DEM was formed using the laser altimeter points, and the match points were intersected with the DEM. This provided an initial estimate for elevation of the control points.

Tie points: Additional match points were added as tie points by using the automatic point measurement (APM) software within SOCET SET (Softcopy Exploitation Tool Set). The image was divided into 9 subareas of an equally spaced 3 by 3 area. APM then locates and measures the tie points in the overlapping images. The triangulation software automatically estimates their ground location based on the camera position and attitude.

Processing

Augmenting LH Systems' SOCET SET digital photogrammetric system [Miller and Walker 1993, Miller and Walker 1995] for photogrammetric mapping of the planets is fairly straightforward when imaging instruments employed by planetary exploration missions behave as framing cameras, such as the CCD array used in Clementine. The necessary adaptations are carried out in two areas. First and fundamentally, geodetic information of the planets and satellites, mapping projection parameters, and camera definitions must be supplied to SOCET SET. Second, an interface between our in-house ISIS (Integrated Software for Imagers and Spectrometers) software system [Eliason 1997, Gaddis et al. 1997, Torson and Becker 1997] and SOCET SET is needed so that the strengths of each system can be easily utilized. (ISIS combines basic capabilities of image processing, analysis and display of 2- and 3-dimensional (multispectral and hyperspectral) data with specialized planetary cartographic functionality.) This interface consists of routines and procedures to import/export image data and associated geometric information; auxiliary data files needed for triangulation; and advanced data products such as DEMs and orthophoto mosaics. Further information on ISIS can be found at the following web site: http://wwwflag.wr.usgs.gov/isis-bin/isis.cgi.

SOCET SET is designed with an internal database directory that stores a suite of static data used to control a variety of SOCET SET functions. These are text files; so adapting SOCET SET to map spherical or near-spherical bodies involves appending planetary reference datums (as radius and eccentricity squared) to the files defining standard Earth reference datums. This is a one-time effort with each new release of SOCET SET and allows the operator selection of a planet figure, by planet or satellite name, at the time a mapping project is being defined. In addition to planetary geodetic information, definitions of grid coordinate systems specific to a planet must be created for subsequent use in SOCET SET. The definitions needed for planetary mapping are appended to a file of existing grid coordinate systems for Earth and consist of a "grid name" (used for operator selection during project creation), the planet radius and eccentricity squared, and the map projection along with its associated parameters. Typical planetary mapping products are produced in Mercator, Transverse Mercator, Lambert Conformal, Polar Stereographic or Sinusoidal map projections. The last data file required by SOCET SET contains camera specifications (i.e., focal length, fiducial coordinates, lens distortion coefficients, etc.). Because of the variety of aerial framing cameras, SOCET SET provides a camera editor where the operator may enter the camera specifications via a GUI (Graphical User Interface) and then save the information to a file in the internal database. For planetary imaging instruments, the focal length and fiducial coordinates are all that is necessary to supply. Lens distortion coefficients are not needed because image processing routines exist in ISIS to digitally remove camera distortions that may have been encountered in certain missions.

Preparing a planetary image for import to SOCET SET requires a few steps in ISIS. First, the native format of the image and support data must be converted using ISIS routines to an ISIS formatted image. Each ISIS image consists of a label area where all the parameters that describe the image are stored as keywords followed by their respective values. Included in the ISIS package are a variety of image processing routines that have been developed for general image enhancement, for mission specific radiometric calibration of imagery, and for the correction of mission specific distortions that may exist, such as camera geometry distortions. Once an image has been enhanced/corrected in ISIS, it is ready for import into SOCET SET.

When importing an image in SOCET SET, known camera position and orientation can be supplied. Camera positions and orientations exist on the labels of ISIS images but in coordinate systems not recognized by SOCET SET. ISIS stores the camera position as a vector in Earth Mean Equatorial (EME) coordinates. EME is an inertial coordinate system (or reference frame) in which the equations of motion for the solar system may be integrated.

EME is specified by the orientation of the Earth's mean equator and equinox at a particular epoch – typically the J2000 epoch. The J2000 epoch is Greenwich noon on January 1, 2000 Barycentric Dynamical Time. (Barycentric Dynamical Time is believed to be in agreement with the time that would be kept by an atomic clock located at the solar system barycenter, i.e., the time at the center of mass around which bodies in the solar system rotate.) For use in SOCET SET, the ISIS camera positions are converted to planetographic coordinates (specifically, longitude and latitude relative to the center of a planet, and height above the planet datum). Attention must be given to the resulting longitude coordinate of the camera position. For many planets, the direction of positive longitude is defined to be positive-west, whereas SOCET SET expects longitudes to be entered as positive-east, such as is the definition on Earth. When positive longitudinal direction conflicts with that of Earth, the longitude signs must be changed upon import to and export from SOCET SET. As for camera orientation angles, these are stored in ISIS as right-ascension, declination and twist (RA, Dec, Twist) angles, which define the transform between EME coordinates and camera coordinates. SOCET SET expects camera orientation angles that define the transformation from ground space (planet surface) to image space, so the ISIS camera orientation angles are converted to the photogrammetrically familiar omega-phi-kappa rotation system.

Once the coordinate system conversions have taken place, the ISIS image is stripped of its labels and imported as a raw-binary file into SOCET SET - along with the known camera position and orientation coordinates. During image import, SOCET SET allows the operator the option to enable atmospheric corrections. For planetary mapping, the operator chooses not to apply atmospheric correction because the default atmospheric correction in SOCET SET is Earth specific; in addition, most planets have little or no atmosphere. (For planets that have an appreciable atmosphere, such as Venus, the planet's specific atmospheric corrections can be incorporated in a custom sensor model. LH Systems offers a Developer's Toolkit that enables their customers to write and incorporate custom sensor models into SOCET SET.)

Other datasets that can be imported/exported between SOCET SET and ISIS consist of image point coordinate and ground point coordinate files used in bundle-block adjustments. (Image triangulation routines in ISIS are targeted for the production of planetary image mosaics – a two dimensional product wherein the overlap requirement between adjacent images can be minimal.) ISIS stores all the image point measurements for a mapping project in a single "match point" file. To identify which image a given image point measurement is on, the match point file lists the "image number", not the filename, of the image. (The image number is stored in the label area of an ISIS image and is unique to each image.) Conversely, SOCET SET is designed to store image point measurements in a separate file for each image in a project, and the actual filenames of the SOCET SET images are used to identify which image a point measurement is on. Importing ISIS match point files into SOCET SET requires mapping the ISIS image numbers to SOCET SET image filenames and creating multiple image point files.

Ground point coordinates for an ISIS project are also stored in a single file, which is the same approach SOCET SET takes. Importing an ISIS ground point file into SOCET SET involves reformatting the ground point information (with attention given to the direction of positive longitude as is the case of camera positions), and adding parameters expected by SOCET SET's MST (Multi Sensor Triangulation), such as weights associated with each point and various flags that indicate whether a point is a control point, tie point or check point. Tie points measured in ISIS for the purpose of making image mosaics can be used as horizontal control in SOCET SET. Typically, tie points measured in ISIS exist between two images only, so to strengthen exterior orientation results in SOCET SET, these points can be propagated to other overlapping images by automatic point measurement techniques in SOCET SET. When laser altimetery data exists for a planet, it can be combined with ISIS tiepoints through interpolation techniques to provide full 3D control for SOCET SET. An altimetry point also can be directly used as 3D control, if the position of the altimetry point can be visually (and reliably) identified on an image.

Modifcations were made to the parameter files used by SOCET SET correlation software in Automatic Point Measurement (APM), Interactive Point Measurement (IPM) and Automatic Terrain Extraction (ATE) modules. Since the Clementine images are small in size, not all the reduced resolution sets that are expected by the correlation software are available. In addition, the search window size needs to be set at an appropriate size for smaller images.

Hardware system: Extraction of the lunar south pole DEMs was primarily performed on a Silicon Graphics Indy XGE, R5000 computer graphics workstation with 126 Mbytes of memory and 476 Mbytes of swap space. For an analytical triangulation consisting of 986 images and 2204 points, run times were about 3.5 hours. To collect 1,764,996 DEM points from 616 stereo models in batch mode took 8 hours of computer time. There were a few days spent manually setting up the DEM boundaries for each model. An advantage is that when the analytical triangulation was recomputed the DEMs could be recollected in batch mode. We are currently transitioning to a Sun Ultra 10 Model 440 with 1 Gbyte of memory and 2 Gbytes of swap space.

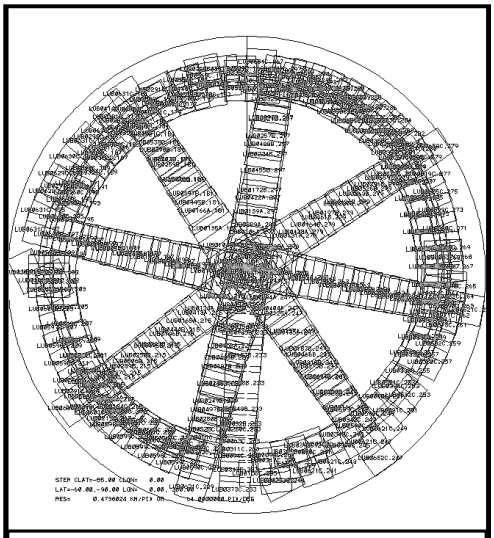

Figure 1 Web layout

Triangulation

For the lunar south pole DEM the dataset consisted of oblique/nadir images from month two, nadir images from month one, and match points used in producing the mosaic which will be used as control points. The images were the UVVIS images with an image center latitude poleward of 60°S and were acquired with the 750 nm filter. There were many tests and experiments done to get the software up and running. For the south polar region, the initial dataset consisted of 6,406 images and 29,386 control points. The image list was reduced to 3,635 images by eliminating the images that were not used in making the global mosaic. All the match points on the selected images were used, and there was no check to see if the control points still fell on two images within the selected set of images. As images were eliminated, some match points ended up on only one image. This dataset was further reduced as explained below.

The dataset of 3,635 images and 29,386 control points was too much information for the analytical triangulation software. An estimate of the amount of memory to perform this adjustment is over 6 Gbytes. The images were therefore broken up into a number of blocks and adjusted in a systematic way. The initial block formed a web over the entire area (Figure 1). This web consisted of an outer circle and eight legs. One leg consists of data from two orbits because there was a break in the circle. The remaining blocks were formed by using two legs of this web and the outer images of the web and filling in the interior with the images to complete the coverage for that block. For the adjustment of the initial block (Figure 1), the camera angles for all images were allowed to be changed by the adjustment process. For the remaining blocks, the camera angles of the images that were part of the initial block were held fixed and the camera angles of the interior images were allowed to change.

First Run: The results of the analytical triangulation for all the blocks showed a root mean square (RMS) of 0.3 pixel with a maximum residual of 2.3 pixels. When DEMs were collected from stereo models the overlap areas had disagreement in the elevation values of 2 - 3 km. The problem was most likely that the stereo models were displaced relative to each other because of the control points. Although the control points were used and adjusted during the process of forming the global mosaic, they were not transferred to other images they overlaid. The majority (3/4) of control points were on two images, the remaining 1/4 of the points were only on one image. There were between 6 and 39 control points per image, with 75% of the images having 15 to 24 control points per image. In order to remove the mismatch between stereo models the control points would have to be propagated to the other images that overlay the points.

SOCET SET has software to automatically transfer points between images. Tests were run with this software and some mismatches did occur and some points failed to transfer. The errors may have been caused by the errors in the pointing geometry (which is why the analytical triangulation needed to be run) or by mismatching features that looked similar. Instead of taking on the enormous job of transferring 29,000 points a decision was made to thin the control points, transfer the thinned points to the other images, add tie points if necessary, and eliminate points that were measured on only one image. Other error sources for point transfer failure were the mismatch in GSD for images collected during month one (GSD μ=142 m, σ=10 m, n=3797) and month two (GSD μ=320 m, σ=50 m, n=1740), and also images near the south pole caused the point transfer software to fail (the reason for this was never determined). The images were thinned to 978 oblique/nadir images from month two.

The control points between 60°S and 75°S were thinned to 50 km between control points, and for control points between 75°S and 90°S they were thinned to 25 km between control points. Nominally, an image would cover 123 km by 92 km and this would allow between 6 and 2 control points per image. The point transfer software was set up to add tie points. This software will divided an image into a 3 by 3 array of cells and check that there was a tie point within the cell. Tie points would automatically be added if there were not any points within the cell. After thinning there were1265 control points. The point transfer software was run and about1200 tie points were added.

Second Run: Now the computer memory could handle the calculations for an analytical triangulation of 978 images and 2400 match points. The process was to run the analytical triangulation, check the points with the largest residuals, and then rerun the analytical triangulation. After a few runs there were no points showing up with obvious blunders. Then all the match points were manually checked to ensure that each point was transferred to all images

that overlaid the point. The point transfer software checked to make sure that all images had a match point within the 3 by 3 array of cells and did not check to make sure that a point was transferred to all possible images.

After a stable solution was found for the analytical triangulation the collection of DEM could begin. The stereo models were based on the oblique and nadir images collected during the same orbit. Although it is possible for SOCET SET to be given a list of images and to automatically derive the DEM from the best pair of images, this software did not work with the Clementine images. The easiest solution was to set up each pair as a model and collect the DEM for that pair. The DEMs collected from images in the same orbit were merged together. Checking the DEMs and editing for errors were done on theses merged DEMs. The computer has slower response times as the volume of the DEM data grows. The DEMs from each orbit were merged together as 8 different sections and finally they were merged together as one DEM.

This DEM was compared with the altimetry data and the topography derived by Dr. Tony Cook [Cook et al. 2000]. Unusual errors were noted. The initial DEM was higher at the outside edges (between 65ºS and 75ºS) than the altimetry data and the data from Cook. Toward the pole, between 90ºS and 80ºS, the data were lower. Upon studying this, it was discovered that the tie points did not change significantly in elevation and (in a very systematic way) the control points had changed significantly in elevation. Graphs were produced that showed the control points had shifted to align with the tie points (Figures 2- 4). The control points had weights of 1,000 for X and Y and 5,000 for Z. The tie points had weights of 10,000 for X, Y and Z. Since the camera angles were adjusted for the global mosaic and the tie points X, Y, and Z ground locations were determined from those camera angles, the difference on the weights of the control and tie points was not large enough and the adjustment stayed at the former adjustment for a spherical moon. To obtain a better solution for the analytical triangulation the weights on the control points Z values would be lower and the camera angles would be reset to the values prior to the adjustment for the global mosaic.

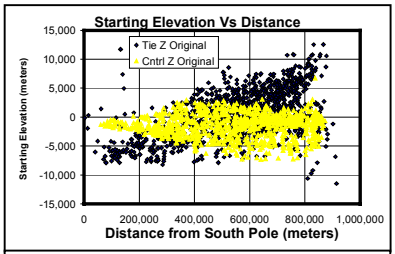

Figure 2 - Starting elevation for match points during the second run.

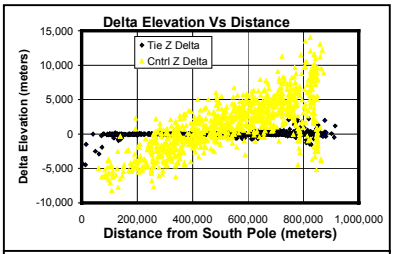

Figure 3 - Change in match points' vertical position after second run.

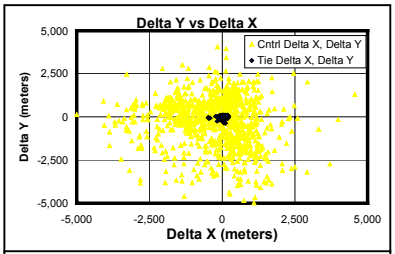

Figure 4 - Change in match points' horizontal position after second run.

Third run: The concept for the next analytical triangulation was to use two passes. The initial pass (Figures 5-7) would be performed with artificially low Z sigma values for the control points whose Z values were based on the Clementine altimetry data. The final pass (Figure 8-10) would use realistic weights and allow the model to adjust. Using this type of weighting would align the results with the Global Mosaic and altimetry data. In addition, during the final pass the results of the initial run would provide better estimates for the tie points ground location.

The sigmas for the control points with elevations based on where the altimetry points were dense (60ºS to 75ºS) were given a Z sigma of 20 m and the other control points were given a Z sigma of 10,000 m. The X and Y sigmas of the control points remained at 1,000 m. For the tie points the sigma values were similar to the previous runs, 10,000 m for X, Y and Z sigma values. The files describing the sensor location and pointing angles were reset to values prior to the adjustment performed for the Global Mosaic. The weights on the control points would bring this initial adjustment into alignment with the horizontal control from the Global Mosaic and align the elevation values to be close to the altimetry data.

The DEMs were recollected and merged together. The DEMs were first merged within an orbit and then the DEMs from different orbits were merged together. The 572 DEMs within an orbit had an RMS error of 836 m and a standard deviation of 155 m. The 50 DEMs that were merged along orbit lines had an RMS error of 391 m and a standard deviation of 351 m. While editing the merged DEMs, a systematic bias was discovered. A model closer to the poles was biased with higher elevation values than an adjacent model farther from the pole. If the models that matched the Clementine altimetry LIDAR were held steady, the DEMs near the pole would have to be lowered and the DEMs from 68°S to 63°S would have to be raised. The merged DEM was overlain with a Clementine south pole mosaic to check the alignment (Figure 11). The contour lines align well with the craters. Some errors can be seen in the concentric rings formed due to a bias in the elevation values.

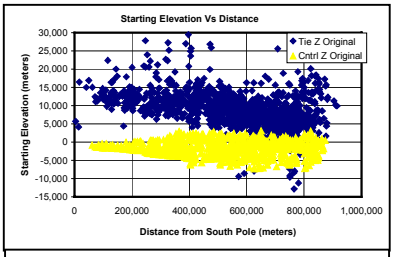

Figure 5 - Starting elevation for match points first pass third run.

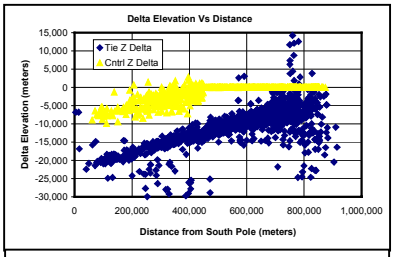

Figure 6 - Change in match points' vertical position after first pass third run.

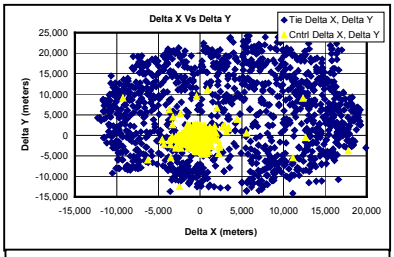

Figure 7 - Change in match points' horizontal position after first pass third run.

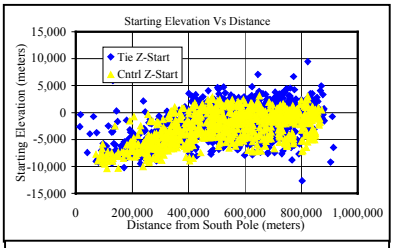

Figure 8 - Starting elevation for match points second pass third run.

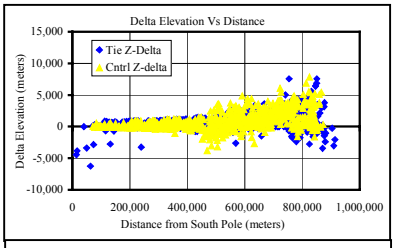

Figure 9 - Change in match points' vertical position after second pass third run.

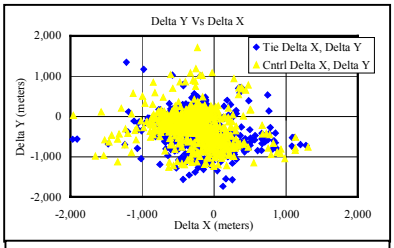

Figure 10 - Change in match points' horizontal position after second pass third

Forth Run: To remove the systematic bias error the DEMs will be adjusted with a least squares program to adjust the elevation values and minimize the error between the DEM and the Clementine altimetry data. The elevation values from this adjustment will be used as estimates for the match point elevation values in another analytical triangulation run. The match point sigmas will be set artificially low and the sigmas on the camera position and attitude will be set high so the position and attitude values will be adjusted. The sigmas for the match point position will be set to a realistic value and the analytical triangulation will be run for a second pass. The hope is that the solution will be stable and that the bias between models within an orbit will be removed. Work is currently under way on modifying the software, and results of the work should be ready for presentation at the conference.

CONCLUSIONS

Topography was collected in areas were the Clementine altimeter was unable to collect data. The topographic data was collected at a post spacing of 1 km. This was an improvement over the Clementine altimeter that was spaced greater than 20 km. The topographic data collected photogrammetrically aligns with the Clementine mosaic. The stereo coverage has some void areas in the lunar south pole area. The missing data can be filled in, were necessary, with the lower resolution altimetry data. This will enable coincident coverage with the boundaries of the Clementine Global Mosaic quadrangle scheme.

Some systematic bias errors exist between the adjacent stereo models used to photogrammetrically derive the topographic data. Some possible causes of these errors include: the distribution of the control points; the overlap between stereo models, in some cases, is very small or non-existent; and errors in the satellite orbit were not completely accounted.

Data collection procedures will be slightly modified for collecting topography over the lunar north pole. The number of match points that are transferred from the ISIS files will increase. This will reduce the number of tie points that are used. In order to tie the model together the higher resolution nadir images will need to be used in areas where the oblique/nadir images do not exist.

ACKNOWLEDGMENTS

Project funding and support is provided by NASA's Research Opportunities in Space Science, Planetary Geology and Geophysics Program. The authors wish to acknowledge the programming support from Trent Hare, and the work of Bonnie Redding and Donna Galuszka in collecting and editing DEMs and match points.

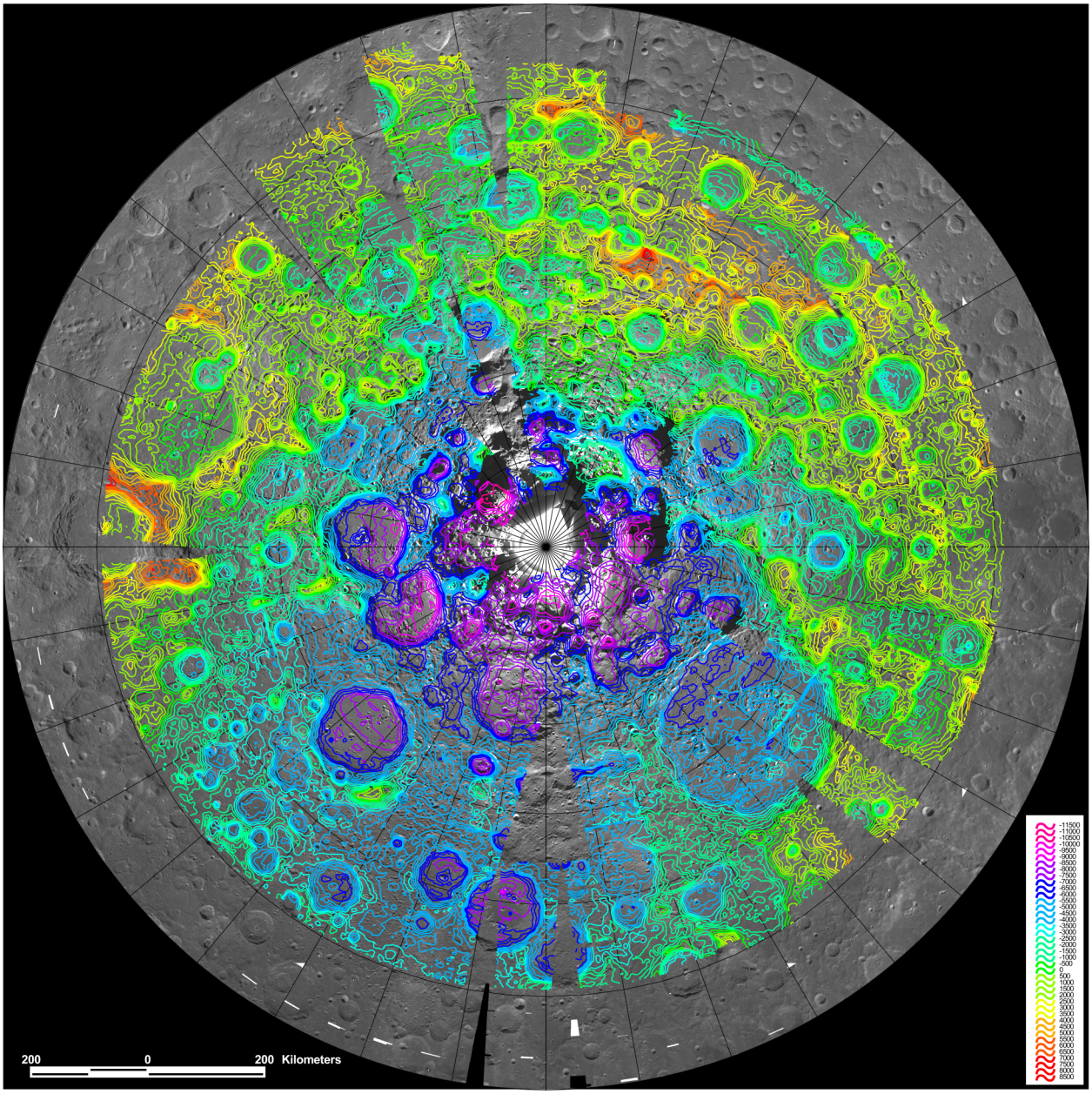

Figure 11. Contour lines for the lunar south pole derived from the DEM collected after the third run. The area shown covers from 60°S to 90°S. Latitude grid lines are spaced 5° and longitude grid lines are spaced 10°. The DEM exhibits errors in the concentric ringlike features that show up in some areas where models do not overlap adequately. Note: This data is still being evaluated and edited. When compared to the Clementine altimetry data the data in figure 11 tends to be 1- 2 km higher at the edge, 65°S. When compared to Tony Cook's data the data in figure 11 tends to be 1- 2 km lower at the pole, 90°S. We are working on adapting the ISIS program EQUALIZE to adjust the errors.

REFERENCES

Cook, A. C., J. Oberst, T. Roatsch, R. Jaumann, and C. Acton, (1996) Clementine imagery: selenographic coverage for cartographic and scientific use, Planet. Space Sci., Vol. 44, No. 10 pages 1135-1148.

Cook, A. C., and M. S. Robinson, (1999) Digital elevation models of the lunar surface. In Workshop on New Views of the Moon II: Understanding the Moon Through the Integration of Diverse Datasets. LPI Contribution No. 980, Lunar and Planetary Institute, Houston.

Cook, A. C.,P. D. Spudis, M. S. Robinson, T. R. Watters, and D. B. J. Bussey, (2000 preprint) Lunar polar topography derived from Clementine stereo imagery, Journal of Geophysical Research, in publication.

Eliason, E.M., (1997) Production of Digital Image Models Using the ISIS System. In Lunar Planet. Sci. XXVIII pages 331-332, Lunar and Planetary Institute, Houston.

Eliason, E.M., A.S. McEwen, M. S. Robinson, E. M. Lee, T. Becker, L. Gaddis, L.A Weller, C. E. Isbell, J. R. Shinaman, T. Duxbury, and E. Malaret (1999) Digital Processing for a Global Multispectral Map of the Moon from the Clementine UVVIS Imaging Instrument. In Lunar Planet. Sci. XXX Abstract 1933, Lunar and Planetary Institute, Houston (CD-ROM).

Gaddis, L. et al. (1997) An Overview of the Integrated Software for Imaging Spectrometers (ISIS) Lunar Planet. Sci. XXVIII pages 387-388, Lunar and Planetary Institute, Houston.

Isbell, C.E., E. M. Eliason, T. Becker, E. M. Lee, (1997) The Clementine Mission: An Archive of a Digital Image Model of the Moon, Lunar Planet. Sci. XXVIII pages 331-332, Lunar and Planetary Institute, Houston.

Isbell, C.E., E. M. Eliason, K. C. Adams, T. L. Becker, A.L Bennett, E. M. Lee, A. S. McEwen, M. S. Robinson, J. R. Shinaman, and L. A. Weller, (1999) Clementine: A Multi-Spectral Digital Image Model Archive of the Moon. In Lunar Planet. Sci. XXX Abstract 1812, Lunar and Planetary Institute, Houston (CD-ROM).

Margot, J.L., D. B. Cambell, R. F. Jurgens, M. A. Slade, N. J. Stacy, (1998) The Topography of the Lunar Polar Regions from Earth-based Radar Interferometry. In Lunar Planet. Sci. XXIX Abstract 1845, Lunar and Planetary Institute, Houston (CD-ROM).

Margot, J.L., D. B. Cambell, R. F. Jurgens, M. A. Slade, (1999A) Locations of Cold Traps and Possible Ice Deposits near the Lunar Poles: A survey Based on Radar Topographic Mapping. In Lunar Planet. Sci. XXX Abstract 1897, Lunar and Planetary Institute, Houston (CD-ROM).

Margot, J.L., D. B. Cambell, R. F. Jurgens, M. A. Slade, (1999B) Topography of the Lunar Poles from Radar Interferometry: A Survey of Cold Trap Locations. Science Vol 284, 4 June 1999, pages 1658 - 1660, www.sciencemag.org.

Miller, S.B. and A. S. Walker, (1993) Further developments of Leica Digital Photogrammetric Systems by Helava, ACSM/ASPRS Annual Convention and Exposition, Technical Papers, Vol. 3, pages 256-263.

Miller, S.B. and A. S. Walker, (1995) Die Entwicklung der digitalen photogrammetrischen Systeme von Leica und Helava. *Zeitschrift für Photogrammetrie und Fernerkundung,* 1/95: pages 4-16.

Nozette, Stewart, et al, (1994), The Clementine Mission to the Moon: Scientific Overview, Science Vol. 266 Pages 1835 - 1839

Oberst, J., T. Roatsch, W. Zhang, A. C. Cook, R. Jaumann, T. Duxbury, F. Wewel, R. Uebbing, F. Scholten, and J. Albertz, (1996)Photogrammetric analysis of Clementine multi-look angle images obtained near Mare Orientale. Planetary and Space Science, 44, 1123–1133.

Rosiek, Mark, R. Kirk, and E. Howington-Kraus, (1999A) Lunar Topographic Maps Derived from Clementine Imagery, In Lunar Planet. Sci. XXX Abstract 1853, Lunar and Planetary Institute, Houston (CD-ROM).

Rosiek, Mark, R. Kirk, R., and E. Howington-Kraus, (1999B) Lunar South Pole Topography Derived from Clementine Imagery. In Workshop on New Views of the Moon II: Understanding the Moon Through the Integration of Diverse Datasets. LPI Contributuion No. 980, Lunar and Planetary Institute, Houston.

Sanders R. G., (1945) Stereoscopy, its History and Uses, Photogrammetric Engineering, Volume XI, Number 2, pages 101-113.

Smith, D. E., M. T. Zuber, G. A. Neumann, and F. G Lemoine, (1997) Topography of the Moon from the Clementine lidar, JGR, Vol. 102, No. E1, Pages 1591-1611

Torson, J. and K. Becker, (1997) A Software Architecture for Processing Planetary Images, Lunar Planet. Sci. XXVIII pages 143-1444, Lunar and Planetary Institute, Houston.

Zuber, M. T., D. E. Smith, F. G. Lemoine, and A. G. Neumann, (1994) The shape and internal structure of the Moon from the Clementine mission. Science, 266, p. 1848–1851.